ISSN: 2277-3754
ISO 9001:2008 Certified
International Journal of Engineering and Innovative Technology (IJEIT)
Volume 3, Issue 2, August 2013

Robust Nonlinear Full State Feedback Control for Autonomous Close Range Rendezvous and Docking of Spacecraft

Daero Lee, Hyochoong Bang

Abstract*— This paper describes a robust nonlinear full state feedback control method that performs the precise translation and rotational maneuvers for autonomous close range rendezvous operations of spacecraft. The primary focus of this study is to design nonlinear state feedback control via the estimated states using extended Kalman filters. The presented nonlinear full state feedback control can achieve robust tracking performances in the presence of external disturbances and parameter uncertainties. This study assumes a Lidar sensor for the relative position and velocity estimations, and a quaternion producing star tracker and a rate-integrating gyro for the chief attitude estimation. The unified state-dependent Riccati equation (SDRE) method is used to design both the position and attitude controllers. The control design is based on a full, 6-degrees of freedom, nonlinear dynamic models, which are manipulated into a linear-like form in which system matrices are given explicitly as a function of the current state. The chaser spacecraft is required to be able to perform large position and attitude maneuvers with sufficient accuracy. Numerical simulation results show that the described control method can obtain good tracking performances to meet the requirements for autonomous proximity operations and docking.

***Index Terms*— Full state feedback control, Autonomous proximity operations and docking, State-dependent Riccati equation method, Extended Kalman filter.**

I. INTRODUCTION

For the past several years, the problems related to rendezvous and docking in space have been developed and applied for many space missions. Rendezvous and docking of spacecraft require adequate modeling, control and estimation of the relative position, velocities, attitude and angular rates. Recently, the subject of automated and autonomous rendezvous and docking has received more attention. Automation is the ability for a spacecraft to operate without human control and inventions, whereas autonomy is the ability for a spacecraft and its on-board systems to perform a function without external support [1]. The level of autonomy is the degree to which the function can be performed by on-board systems and the crew without ground systems support or support from other spacecraft. This study for autonomy deals with on-board navigation and control systems. A rendezvous mission can be divided into a number of major phases: launch, phasing, far range rendezvous, close range rendezvous and mating (docking or berthing) [2]. Each phase has its objectives and end conditions. In general, the phase is divided into two sub phases: a preparatory phase leading to the final approach corridor, often called ‘closing’, and a final approach phase leading to the docking conditions. No distinction can be made between a closing and a final approach sub phase in the V-bar approach since the direction of the motion remains the same and no change of sensor type occurs. This study considers the phase of close range rendezvous with a V-bar approach. The objectives of the closing phase are to reduce the range to the target and to achieve conditions allowing for the acquisition of the final approach corridor. The objective of the final approach phase is to achieve a docking condition in terms of positions and velocities, and of relative attitude and angular rates. For a soft docking, the relative position and rate, as well as relative attitude, should be very small. This study assumes precise onboard sensor systems capable of providing range, bearing angles and relative attitude between two spacecraft.

In order to achieve the robustness in the translation and rotational maneuvers, the nonlinear full state feedback control via the state estimation has been designed. A kinematic and a dynamic equation of motions, which are highly nonlinear, are required to fully describe the translational and rotational motions of a rigid spacecraft. Thus, a linear controller design for the spacecraft maneuvers may not be suitable and lead to a substantially higher fuel cost, especially when long-term maneuvers are required in the external disturbances, or a large position or angle maneuvers are required. Various nonlinear control techniques have been investigated in the past to address this problem. Among the many control techniques, the state-dependent Riccati equation (SDRE) method has emerged as a general design method that provides systematic and effective means of designing nonlinear controllers, observers, and filters since the mid-90’s. It also has been widely used for aerospace engineering that requires real time control systems [3]-[8]. For instance, Stansbery and Cloutier [3] proposed the SDRE nonlinear regulation to control the position and attitude of a spacecraft in the proximity of a tumbling target. Xin and Balakishnan [4] combined a SDRE with a neural network based extra control to design a robust spacecraft attitude controller in the presence of inertia uncertainties. Menon et al. [5] demonstrated the feasibility of implementing the SDRE technique in real-time using commercial, off-the-shelf computers. The SDRE method is an extension of the linear quadratic regulator (LQR) problem for a linear system. In the SDRE method, nonlinear equations of motion are represented in a linear-like form, called the state-dependent coefficient (SDC) form, which corresponds to the system matrix expressed explicitly as a function of the state element. In doing so, the SDRE method fully captures

ISSN: 2277-3754
ISO 9001:2008 Certified
International Journal of Engineering and Innovative Technology (IJEIT)
Volume 3, Issue 2, August 2013

the nonlinearities of the system, transforming the nonlinear system to a non-unique linear structure through the SDC parameterization and minimizing cost function by having a quadratic-like structure. An algebraic Riccati equation (ARE) is then solved on-line to give the suboptimal control law. Unlike the LQR method, the coefficients of this ARE vary along the given points in state space. Most of the dynamic systems can be directly parameterized in a SDC form. However, there are systems that prevent a direct SDC parameterization and require conformation to the proper structure and conditions due to the presence of state-independent terms or state-dependent terms that exclude the origin. A systematic and effective design of nonlinear feedback controllers via this method is described in Ref. [8]. For spacecraft proximity operations and docking problems, nonlinear relative motion dynamics, including external disturbances, is used for the SDRE control formulation [9], [10].

Many controls have been developed from the selected plant model. They may work successfully in their selected control plant. However, the control may not be able to cope with the presence of parametric uncertainty, measurement noise and external disturbances for long-duration missions. For instance, disturbance that exists in spacecraft proximity operations and docking problems can often cause unsatisfactory performance in a controller that is designed without taking them account. In addition, the state feedback in a control design cannot be implemented in practice since all the states are not usually available as measurements. Thus, these important issues should be considered to develop a robust and implementable control algorithm. A practical strategy for designing an efficient control system using available noisy measurements can be the use of a filter to estimate the state and design a state feedback control via the estimated states. It may be desirable to design the controller and the state estimator separately, even in the confirmatively established separation principle [11],[12]. The most common way of applying the Kalman filter to a nonlinear system is in the form of the extended Kalman filter (EKF). An extended Kalman filter (EKF) has been widely used in many applications where the mathematical model is nonlinear, but where linearization and truncation to first-order terms are presumed valid. Having estimated the states used, we may then use the estimated state for feedback purposes, designing a feedback gain as if all the states were measurable. The combination of the SDRE control and the EKF is then a dynamic controller similar to those used in classical control, such as linear quadratic Gaussian control (LQG) [15]. In this study, the SDRE control method and the EKF filters were designed separately to yield the desired closed-loop plant behavior and the estimator behavior with the implicit assumption that a separation theory still holds.

To add realism, an imaginary "truth" plant is employed by adding external disturbance forces and torques, modeled as zero-mean Gaussian white-noise process to the selected systems for control designs, respectively. The imaginary truth plants are then used to generate the true relative position, velocity and the chaser quaternions when the controls are applied. They are then compared with the states from controllers. The selected plants for the control designs also include the external disturbances that violate the constraints for SDC. Thus, the SDRE controls are formulated in the presence of state-independent and state-dependent terms, requiring special manipulation, instead of a direct SDC parameterization. The predefined time-varying states of the target are propagated. The control problem to track the desired states is formulated as the optimal tracking problem. The estimated states using the EKF filter can offer realistic state variation due to external disturbances and the uncertainties of plant parameters. The estimated states are then used to design state feedback controls.

Thus, the unified nonlinear full state feedback controllers based on the combination of the SDRE control and the EKF filters perform well under external disturbances and large uncertainties of the plant parameters. In addition, they demonstrate excellent tracking performances required for close range rendezvous and dock phases through six-degrees-of freedom simulations. The simulation results show that the controllers can carry out the close range rendezvous successfully and meet the conditions for docking phases.

II. PROBLEM FORMULATION

In this study, we considered an autonomous spacecraft mission for autonomous close range rendezvous between two spacecraft. The objective of the control design is to have the chaser tracked the predefined reference trajectory towards the docking port of the target, which is supposed to be at the origin of the inertial frame $\mathbf{N}_I\{\mathbf{n}_x,\mathbf{n}_y,\mathbf{n}_z\}$ and the rotating Hill frame $\mathbf{H}\{\mathbf{e}_R,\mathbf{e}_T,\mathbf{e}_N\}$. It was also desired to have the chaser body-fixed frame $\mathbf{B}_c\{\mathbf{b}_{c_x},\mathbf{b}_{c_y},\mathbf{b}_{c_z}\}$ aligned with the target body frame $\mathbf{B}_t\{\mathbf{b}_{t_x},\mathbf{b}_{t_y},\mathbf{b}_{t_z}\}$. The unite vector $\mathbf{e}_R$ is aligned in a radial direction and $\mathbf{e}_N$ is aligned with the orbit angular momentum, whereas $\mathbf{e}_T$ is aligned along the direction of the track and completes the triad. The inertial coordinate system and the Hill frame, as well as the target and chaser body-fixed coordinate systems, are illustrated in Fig. 1.

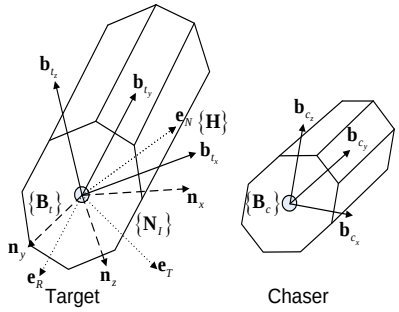

Fig. 1. Target and chaser body-fixed frames, Hill and inertial frames

ISSN: 2277-3754
ISO 9001:2008 Certified
International Journal of Engineering and Innovative Technology (IJEIT)
Volume 3, Issue 2, August 2013

The chaser is required to maneuver a predefined desired trajectory from the target and achieve the attitude and angular rate of the target simultaneously. The relative position vector $\boldsymbol{\rho}$ is expressed in the Hill rotating frame components as $\boldsymbol{\rho} = \begin{bmatrix} x & y & z \end{bmatrix}^T$. The inertial target position is expressed through the vector $\mathbf{r}_t$ while the chaser position is given by $\mathbf{r}_c$. The subscripts t and c denote the target and the chaser, respectively. The translational motion of the chaser is described by the relative orbital equations of motion. A complete derivation of the relative equations of motion with no disturbances for an eccentric orbit is described in [12]. It uses an assumption no disturbances have been made on the spacecraft. Thus, the Keplerian motion assumption in the orbital equations of motion is correct. However, the really existing disturbances in the close range rendezvous need to be considered for accurate dynamic modeling. The disturbances are the relative effects of the Earth's oblateness and aerodynamic drag, which are dominant in low Earth orbit (LEO) among the various perturbation sources. The perturbing acceleration by the effect of Earth oblateness of J_2 term [13] is described in terms of its components in the Hill frame and is given by

$$\mathbf{a}_{J_2} = \frac{-3\mu J_2 R_e^2}{r^4}\left[\begin{array}{l}\left(\frac{1}{2} - \frac{3\sin^2 i \sin\theta}{2}\right)\mathbf{e}_R + \left(\sin^2 i \sin\theta\cos\theta\right)\mathbf{e}_T \\ +\left(\sin i \sin\theta \cos i\right)\mathbf{e}_N\end{array}\right] \quad (1)$$

where R_e is the radius of the Earth, i is the inclination angle, and θ is the argument of latitude. The relative perturbing acceleration due to the effect of Earth's oblateness by J_2 term is then

$$\Delta\mathbf{a}_{J_2} = \mathbf{a}_{J_2}\left(r_c, i_c, \theta_c\right) - \mathbf{a}_{J_2}\left(r_t, i_t, \theta_t\right) \quad (2)$$

When the perturbing acceleration is computed, the precise target orbit is assumed to be known from the on-board navigation system of the target. Then, the chaser orbit is computed using the relative orbit with the target orbit. The atmospheric drag perturbation [14] is expressed in an ECI coordinate and is then transformed into the Hill frame using the appropriate direction cosine matrix to obtain

$$\mathbf{a}_d = -\frac{1}{2}\rho\left(\frac{c_d A}{m}\right)|\mathbf{V}_r|\mathbf{V}_r \quad (3)$$

Here, ρ is the atmospheric density and follows the exponential model, while c_d is the drag coefficient that depends on the shape and surface. Also, A is the reference cross-sectional area of the spacecraft, m is the spacecraft mass and $\mathbf{V}_r$ is the spacecraft velocity vector relative to the atmosphere in the inertial coordinate. The relative perturbation by the effect of atmospheric drag, expressed in the Hill frame, is then given by

$$\Delta\mathbf{a}_D = C\left(\mathbf{a}_d\left(\rho_c, c_{d_c}, A_c, m_c, \mathbf{V}_{r_c}\right) - \mathbf{a}_D\left(\rho_t, c_{d_t}, A_t, m_t, \mathbf{V}_{r_t}\right)\right) \quad (4)$$

where C is the 3-1-3 rotation sequence $C = C_3(\theta_t)C_1(i_t)C_3(\Omega_t)$ for transformation from the Earth-centered inertial (ECI) coordinate to the local-vertical-local-horizontal (LVLH) Hill frame. Then, the sum of the relative perturbations by the effects of the Earth's oblateness and atmospheric drag is

$$\Delta\mathbf{a} = \Delta\mathbf{a}_{J_2} + \Delta\mathbf{a}_D \quad (5)$$

Thus, the relative equation of motions, including the sum of the relative perturbations for translational maneuvers when the control force is applied, is given by

$$\ddot{x} - 2\dot{f}\left(\dot{y} - y\frac{\dot{r}_t}{r_t}\right) - x\dot{f}^2 - \frac{\mu}{r_t^2} = -\frac{\mu}{r_c^3}\left(r_t + x\right) + \Delta a_x + \frac{F_x}{m(t)} \quad (6a)$$

$$\ddot{y} + 2\dot{f}\left(\dot{x} - x\frac{\dot{r}_t}{r_t}\right) - y\dot{f}^2 = -\frac{\mu}{r_c^3}y + \Delta a_y + \frac{F_x}{m(t)} \quad (6b)$$

$$\ddot{z} = -\frac{\mu}{r_c^3}z + \Delta a_z + \frac{F_x}{m(t)}, \quad r_c = \sqrt{\left(r_t + x\right)^2 + y^2 + z^2} \quad (6c)$$

where μ is the gravitational parameter and f represents the true anomaly of the target. Also, F_x, F_y and F_z are the applied control force components of $\mathbf{F}_H \in \Re^3$ in the Hill frame and $m(t)$ is the time-varying mass of the chaser. The applied control forces, $\mathbf{F}_H$, can be transformed to the force $\mathbf{F}_c \in \Re^3$ in the chaser body-fixed frame using the target orbit and the chaser attitude, while $\Delta a_x, \Delta a_y$ and Δa_z are the components of $\Delta\mathbf{a}$.

To fully describe the rotational maneuvers of the rigid body chaser, kinematic equations and dynamic equations of motion are required. The kinematic equation for attitude is

$$\dot{\mathbf{q}}_c = \frac{1}{2}\Omega(\boldsymbol{\omega}_c)\mathbf{q}_c \quad (7)$$

and the dynamic equation is

$$I_c\dot{\boldsymbol{\omega}}_c = -\left[\boldsymbol{\omega}_c \times\right]I_c\boldsymbol{\omega}_c + \boldsymbol{\Gamma}_c \quad (8)$$

where $I_c \in \Re^{3\times 3}$, $\boldsymbol{\omega}_c = \begin{bmatrix}\omega_{c_1} & \omega_{c_2} & \omega_{c_3}\end{bmatrix}^T$ and $\boldsymbol{\Gamma}_c \in \Re^3$ are the moment of inertia, angular velocity and control torque of the chaser, respectively. Note that they are defined in the chaser's body-fixed frame. The four elements of the quaternion are defined by

$$q_i = \hat{\mathbf{e}}\sin(\vartheta/2), i = 1,2,3 \quad (9a)$$

$$q_4 = \cos(\vartheta/2) \quad (9b)$$

where $\hat{\mathbf{e}}$ is the Euler axis of rotation and ϑ is the Euler-axis rotation angle. $\left[\boldsymbol{\omega}_c \times\right]$ and $\Omega(\boldsymbol{\omega}_c)$ are defined as, respectively

ISSN: 2277-3754
ISO 9001:2008 Certified
International Journal of Engineering and Innovative Technology (IJEIT)
Volume 3, Issue 2, August 2013

$$[\boldsymbol{\omega}_c \times] = \begin{bmatrix} 0 & -\omega_{c_z} & \omega_{c_y} \\ \omega_{c_z} & 0 & -\omega_{c_x} \\ \omega_{c_y} & \omega_{c_x} & 0 \end{bmatrix} \quad (10)$$

$$\Omega(\boldsymbol{\omega}_c) = \begin{bmatrix} -[\boldsymbol{\omega}_c \times] & \boldsymbol{\omega}_c \\ -\boldsymbol{\omega}_c^T & 0 \end{bmatrix} \quad (11)$$

As the sum of relative disturbance accelerations for the accurate modeling of translational maneuvers is included, the sum of relative disturbance torques is also included for the accurate modeling of rotational maneuvers. An object in LEO does not experience the same gravitational pull on all parts of its body. This study models only the gravity-gradient torque and the torque due to atmospheric drag that are dominant in LEO. The effects of the gravitational field are not uniform over an asymmetry body in space, creating a gravitational torque about the body's center of mass. The gravity-gradient torque expressed in a vector/dyadic form [10], $\mathbf{T}_g \in \Re^3$, is given as

$$\mathbf{T}_g = 3\frac{\mu}{r_c^3}\mathbf{e}_r \times I_c \cdot \mathbf{e}_r \quad (12)$$

Then, $\mathbf{e}_r$ can be expressed in terms of the basis vector of the body-fixed frame B of a spacecraft relative to the Hill frame as

$$\mathbf{e}_r = C_{12}^{B/H}\mathbf{b}_x + C_{22}^{B/H}\mathbf{b}_y + C_{32}^{B/H}\mathbf{b}_z \quad (13)$$

The direction cosine matrix $C^{B/H}$ can be expressed using successive rotations with the inertial frame N_I through

$$C^{B/H} = C^{B/N_I}C^{N_I/H} \quad (14)$$

The gravity-gradient torque $\mathbf{T}_g \in \Re^3$ becomes

$$\mathbf{T}_g = 3\frac{\mu}{r_c^3}\begin{bmatrix} 0 & -C_{32}^{B/H} & C_{22}^{B/H} \\ C_{32}^{B/H} & 0 & -C_{12}^{B/H} \\ -C_{22}^{B/H} & C_{12}^{B/H} & 0 \end{bmatrix}\begin{bmatrix} I_{c_{11}} & I_{c_{12}} & I_{c_{13}} \\ I_{c_{21}} & I_{c_{22}} & I_{c_{23}} \\ I_{c_{31}} & I_{c_{32}} & I_{c_{33}} \end{bmatrix}\begin{bmatrix} C_{12}^{B/H} \\ C_{22}^{B/H} \\ C_{32}^{B/H} \end{bmatrix} \quad (15)$$

The interaction of the upper atmosphere molecules with the satellite's surface introduces an atmospheric drag torque $\mathbf{T}_d \in \Re^3$, which is given by

$$\mathbf{T}_d = C(C_p - C_m) \times -\frac{1}{2}\rho\left(\frac{C_D A}{m}\right)\|\mathbf{V}_r\|\mathbf{V}_r \quad (16)$$

where C_p, C_m are the position vectors of the center of pressure and the center of mass in the ECI coordinate, respectively.

$$I_c\dot{\boldsymbol{\omega}}_c = -[\boldsymbol{\omega}_c \times]I_c\boldsymbol{\omega}_c + \boldsymbol{\Gamma}_c + (\mathbf{T}_g + \mathbf{T}_d) \quad (17)$$

In sum, the chaser spacecraft maneuvers to perform close range rendezvous through the control forces, $\mathbf{F}_H \in \Re^3$, and control torques, $\boldsymbol{\Gamma}_c \in \Re^3$. The nonlinear equations of the spacecraft kinematics and dynamics, including disturbance forces and torques, can be written in a state space form, $\dot{\mathbf{x}} = \boldsymbol{f}(\mathbf{x}) + B(\mathbf{x})\mathbf{u}$, respectively.

$$\begin{bmatrix} \dot{\boldsymbol{\rho}} \\ \ddot{\boldsymbol{\rho}} \end{bmatrix} = \begin{bmatrix} \dot{x} \\ \dot{y} \\ \dot{z} \\ \ddot{x} \\ \ddot{y} \\ \ddot{z} \end{bmatrix} = \begin{bmatrix} \dot{x} \\ \dot{y} \\ \dot{z} \\ 2\dot{f}\left(\dot{y} - y\frac{\dot{r}_t}{r_t}\right) + x\dot{f}^2 + \frac{\mu}{r_t^2} - \frac{\mu}{r_c^3}(r_t + x) + \Delta a_x \\ -2\dot{f}\left(\dot{x} - x\frac{\dot{r}_t}{r_t}\right) + y\dot{f}^2 - \frac{\mu}{r_c^3}y + \Delta a_y \\ -\frac{\mu}{r_c^3}z + \Delta a_z \end{bmatrix} + \begin{bmatrix} 0_{3\times3} & 0_{3\times3} \\ \frac{1}{m(t)}0_{3\times3} & 0_{3\times3} \end{bmatrix}\begin{bmatrix} 0_{3\times1} \\ \mathbf{F}_H \end{bmatrix} \quad (18)$$

$$\begin{bmatrix} \dot{\mathbf{q}}_c \\ \dot{\boldsymbol{\omega}}_c \end{bmatrix} = \begin{bmatrix} \frac{1}{2}\Omega(\boldsymbol{\omega}_c)\mathbf{q}_c \\ -I_c^{-1}[\boldsymbol{\omega}_c \times]I_c\boldsymbol{\omega}_c + I_c^{-1}\mathbf{T}_g + I_c^{-1}\mathbf{T}_d \end{bmatrix} + \begin{bmatrix} 0_{4\times3} \\ I_c^{-1} \end{bmatrix}\boldsymbol{\Gamma}_c \quad (19)$$

Thus, the nonlinear controllers are designed using Eqs. (18) and (19) by the SDRE method. The extended filters are then designed to replace the control state with the estimated state. Though a general separation principle for nonlinear systems is not available for nonlinear systems, its feasibility is often assumed for all practical purposes. The architecture of the controller and the filter combination is schematically described in Fig. 2.

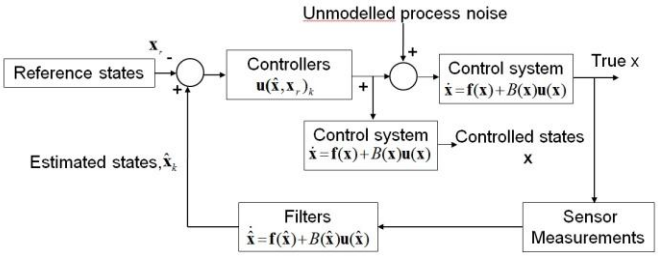

Fig. 2. Architecture of the controller and the filter combination

Remark The true states of the dynamic system in spacecraft rendezvous and docking may be obtained in the presence of many known and unknown external disturbances. If the states can guarantee the estimation accuracy condition for control purposes via the filter, they can be replaced with the control response to compute the control. As the state value approach the true state value via the filter and with the help of precision sensors, all states of the control state $\mathbf{x}$, the true state, $\mathbf{x}_{true}$, and the filtered state, $\hat{\mathbf{x}}$ get similar depending on the estimation accuracy. Thus, the following relation can be achieved as follows. The true state $\mathbf{x}_{true} \approx$ the control state, $\mathbf{x} \approx$ the filtered state, $\hat{\mathbf{x}}$.

III. THE SDRE METHOD

The autonomous, infinite horizon, nonlinear problem for minimizing the performance index is considered

ISSN: 2277-3754
ISO 9001:2008 Certified
International Journal of Engineering and Innovative Technology (IJEIT)
Volume 3, Issue 2, August 2013

$$J = \frac{1}{2}\int_0^\infty \left[\mathbf{x}^T Q(\mathbf{x})\mathbf{x} + \mathbf{u}^T R(\mathbf{x})\mathbf{u}\right] dt \quad (20)$$

with respect to the state $\mathbf{x}$ and control $\mathbf{u}$, which are subject to the nonlinear differential constraints:

$$\dot{\mathbf{x}} = \mathbf{f}(\mathbf{x}) + B(\mathbf{x})\mathbf{u} \quad (21)$$

where $Q(\mathbf{x}) \geq 0$ and $R(\mathbf{x}) > 0$ for all $\mathbf{x}$ and $\mathbf{f(0) = 0}$. The SDRE control method provides an approximate nonlinear feedback solution for the above problem. The SDRE design technique consists of the following steps. First, the direct parameter method is used to bring the nonlinear equation into state-dependent coefficients (SDC) form, which is a linear-like structure.

$$\dot{\mathbf{x}} = A(\mathbf{x})\mathbf{x} + B(\mathbf{x})\mathbf{u} \quad (22)$$

For the system to be controllable, the matrices $A(\mathbf{x})$ and $B(\mathbf{x})$ evaluated all possible states and should meet the controllability condition. To obtain a valid solution of the SDRE, the pair $\{A(\mathbf{x}), B(\mathbf{x})\}$ has to be point wise stabilized in the linear sense so that for all $\mathbf{x}$ in the domain of interest, a feasible (i.e., positive definite) solution may be obtained. Second, the SDRE is solved.

$$P(\mathbf{x})A(\mathbf{x}) + A(\mathbf{x})^T P(\mathbf{x}) - P(\mathbf{x})B(\mathbf{x})R(\mathbf{x})^{-1}B(\mathbf{x})^T P(\mathbf{x}) + Q(\mathbf{x}) = 0 \quad (23)$$

Where, $P(\mathbf{x})$ is state dependent, positive definite for $\mathbf{x} \neq \mathbf{0}$. Third, the nonlinear feedback controller equation is constructed.

$$\mathbf{u}(\mathbf{x}) = -R^{-1}(\mathbf{x})B^T(\mathbf{x})P(\mathbf{x})\mathbf{x}(t) \quad (24)$$

To perform the following command, the SDRE controller can be implemented as an integral servomechanism, as demonstrated in [3]. The control state $\mathbf{x}$ is desired to track the reference commands, $\mathbf{x}_r(t)$. The integral servo controller is modified without an integral state and is then given by

$$\mathbf{u}(\mathbf{x}) = -R^{-1}(\mathbf{x})B^T(\mathbf{x})P(\mathbf{x})\left[\mathbf{x}(t) - \mathbf{x}_r(t)\right] \quad (25)$$

For the desired performance objectives using the control in Eq. (25), the weight matrices $Q(\mathbf{x})$ and $R(\mathbf{x})$ can be appropriately tuned.

IV. SDRE Controller Design

The objective of the control design for translational maneuvers is to have the chaser position and velocity, $\boldsymbol{\rho}$ and $\dot{\boldsymbol{\rho}}$, track the reference commands, $\boldsymbol{\rho}_r$ and $\dot{\boldsymbol{\rho}}_r$, in the rotating Hill frame. The objective of the control design for rotational maneuvers is to have the chaser body-fixed frame $\mathbf{B}_c\{\mathbf{b}_{c_1}, \mathbf{b}_{c_2}, \mathbf{b}_{c_3}\}$ coincide with the target body-fixed frame $\mathbf{B}_t\{\mathbf{b}_{t_1}, \mathbf{b}_{t_2}, \mathbf{b}_{t_3}\}$.

A. Translational Maneuver

The state vector for the translational maneuver was chosen to be

$$\mathbf{x}_T = \begin{bmatrix} x & y & z & \dot{x} & \dot{y} & \dot{z} \end{bmatrix}^T, \mathbf{x}_T \in \Re^6 \quad (26)$$

The general form of Eq. (21) for translational maneuver is given by

$$\dot{\mathbf{x}}_T = \mathbf{f}(\mathbf{x}_T) + B_T(\mathbf{x}_T)\mathbf{u}_F \quad (27)$$

where $\mathbf{u}_F$ is the control force. The SDC form is then given by

$$\dot{\mathbf{x}}_T = A_T(\mathbf{x}_T)\mathbf{x}_T + B_T\mathbf{u}_F \quad (28)$$

The cost function to be minimized for the translational maneuvers is given by

$$J = \frac{1}{2}\int_0^\infty \left[\mathbf{x}_T{}^T Q_T \mathbf{x}_T + \mathbf{u}_F^T R_T \mathbf{u}_F\right] dt \quad (29)$$

The nonlinear relative motion dynamics in Eq. (18) is written in a linear-like form in Eq. (28) through the state-dependent coefficient (SDC) parameterization. However, there is the presence of state-independent terms, referred to as the bias term, which is the requirement that $\mathbf{f(0) = 0}$ in condition [8] for direct SDC parameterization is violated. Using a property where the approaching speed of spacecraft never goes to zero, the bias term in Eq. (18) can then be parameterized in a SDC form. The particular chosen $A_T(\mathbf{x}_T)$ for this application is given by

$$\begin{bmatrix} 0 & 0 & 0 & 1 & 0 & 0 \\ 0 & 0 & 0 & 0 & 1 & 0 \\ 0 & 0 & 0 & 0 & 0 & 1 \\ (\dot{f}^2 - \frac{\mu}{r_c^3}) & (-2\dot{f}\frac{\dot{r}_t}{r_t}) & 0 & (2\dot{f} + (\frac{\mu}{r_t^2} - \frac{\mu}{r_c^3}r_t + \Delta a_x)\dot{x}/v) & (\frac{\mu}{r_t^2} - \frac{\mu}{r_c^3}r_t + \Delta a_x)\dot{y}/v & (\frac{\mu}{r_t^2} - \frac{\mu}{r_c^3}r_t + \Delta a_x)\dot{z}/v \\ (2\dot{f}\frac{\dot{r}_t}{r_t}) & (\dot{f}^2 - \frac{\mu}{r_c^3}) & 0 & (-2\dot{f} + \Delta a_y\dot{x}/v) & (\Delta a_y\dot{y}/v) & (\Delta a_y\dot{z}/v) \\ 0 & 0 & (-\frac{\mu}{r_c^3}) & (\Delta a_z\dot{x}/v) & (\Delta a_z\dot{y}/v) & (\Delta a_z\dot{z}/v) \end{bmatrix} \quad (30)$$

Where v is the speed of spacecraft. The control distribution matrix is

$$B_T(\mathbf{x}_T) = \begin{bmatrix} 0_{3\times3} \\ \frac{1}{m(t)} I_{3\times3} \end{bmatrix} \quad (31)$$

The state weight matrix for the performance index in Eq. (29) is given by

$$Q_T = 10^4 \begin{bmatrix} I_{3\times3} & 0_{3\times3} \\ 0_{3\times3} & 0_{3\times3} \end{bmatrix} \quad (32)$$

The control weight matrix in Eq. (29) is given by

$$R_T = I_{3\times3} \quad (33)$$

ISSN: 2277-3754
ISO 9001:2008 Certified
International Journal of Engineering and Innovative Technology (IJEIT)
Volume 3, Issue 2, August 2013

The control force to track the desired position and velocity is then obtained using Eq. (25)

$$\mathbf{u}_F(\mathbf{x}_T) = -R_T^{-1} B_T^T(\mathbf{x}_T) P(\mathbf{x}_T)\left[\mathbf{x}_T(t) - \mathbf{x}_{T_r}(t)\right] \quad (34)$$

Where $\mathbf{x}_{T_r}(t)$ is the reference commands using the Clohessy-Wiltshire (CW)'s linear impulse rendezvous and station keeping conditions.

B. Rotational Maneuver

The state vector for the rotational maneuvers was chosen to be

$$\mathbf{x}_R = [\mathbf{q} \quad \boldsymbol{\omega}]^T, \mathbf{x}_R \in \Re^7 \quad (35)$$

The general form of Eq. (22) for rotational maneuver is given by

$$\dot{\mathbf{x}}_R = \mathbf{f}(\mathbf{x}_R) + B_R \mathbf{u}_\Gamma \quad (36)$$

where $\mathbf{u}_\Gamma$ is the control torque. The SDC form is then given by

$$\dot{\mathbf{x}}_R = A_R(\mathbf{x}_R)\mathbf{x}_R + B_R \mathbf{u}_\Gamma \quad (37)$$

The cost function to be minimized for the rotational maneuvers is given by

$$J = \frac{1}{2}\int_0^\infty \left[\mathbf{x}_R{}^T Q_R \mathbf{x}_R + \mathbf{u}_\Gamma^T R_R \mathbf{u}_\Gamma\right] dt \quad (38)$$

The state space form in Eq. (19) is written in a linear-like form in Eq. (37) through the SDC parameterization. Like the SDC parameterization in Eq. (18), there is also a bias term in Eq. (19) that prevents meeting the requirement that **f(0) = 0** in the condition. Using a property where the magnitude of the quaternion is 1, the bias term in Eq. (19) can then be parameterized in a SDC form. The particular chosen $A_R(\mathbf{x}_R)$ for this application is then given by

$$\begin{bmatrix}
\varepsilon_\omega & 0 & 0 & 0 & 0.5q_{c_4} & -0.5q_{c_3} & 0.5q_{c_2} \\
0 & \varepsilon_\omega & 0 & 0 & 0.5q_{c_3} & 0.5q_{c_4} & -0.5q_{c_1} \\
0 & 0 & \varepsilon_\omega & 0 & -0.5q_{c_2} & 0.5q_{c_1} & 0.5q_{c_4} \\
0 & 0 & 0 & \varepsilon_\omega & -0.5q_{c_1} & -0.5q_{c_2} & -0.5q_{c_3} \\
a_{5,4}q_{c_1}/\|\mathbf{q}_c\| & a_{5,4}q_{c_2}/\|\mathbf{q}_c\| & a_{5,4}q_{c_3}/\|\mathbf{q}_c\| & a_{5,4}q_{c_4}/\|\mathbf{q}_c\| & 0 & 0 & 0 \\
a_{6,4}q_{c_1}/\|\mathbf{q}_c\| & a_{6,4}q_{c_2}/\|\mathbf{q}_c\| & a_{6,4}q_{c_3}/\|\mathbf{q}_c\| & a_{6,4}q_{c_4}/\|\mathbf{q}_c\| & 0 & 0 & 0 \\
a_{7,4}q_{c_1}/\|\mathbf{q}_c\| & a_{7,4}q_{c_2}/\|\mathbf{q}_c\| & a_{7,4}q_{c_3}/\|\mathbf{q}_c\| & a_{7,4}q_{c_4}/\|\mathbf{q}_c\| & 0 & 0 & 0
\end{bmatrix} \quad (39)$$

Where ε_ω is added to the quaternion kinematics to avoid the uncontrollability and obtain the solution of the algebraic Ricatti equation since the system is prone to be uncontrollable. $a_{5,4}$, $a_{6,4}$ and $a_{7,4}$ are equal to three elements of the 3×1 vector $-(I_c^{-1}\boldsymbol{\omega}_c{}^\times I_c \boldsymbol{\omega}_c)/q_{c_4}$, respectively. $\|\mathbf{q}_c\|$ is also the magnitude of the quaternion of the chaser. The control distribution matrix is

$$B_T(\mathbf{x}_T) = \begin{bmatrix} 0_{4\times3} \\ I_c^{-1} \end{bmatrix} \quad (40)$$

The state weighting matrix for the performance index in Eq. (38) is given by

$$Q_R = \begin{bmatrix} 5\times10^2 I_{3\times3} & 0_{3\times3} \\ 0_{3\times3} & 0_{3\times3} \end{bmatrix} \quad (41)$$

The control weighting matrix in Eq. (38) is given by

$$R_R = I_{3\times3} \quad (42)$$

The control torque to coincide with the desired attitude is then obtained using Eq. (25)

$$\mathbf{u}_\Gamma(\mathbf{x}_R) = -R_R^{-1} B_R^T(\mathbf{x}_R) P(\mathbf{x}_R)\left[\mathbf{x}_R(t) - \mathbf{x}_{R_r}(t)\right] \quad (43)$$

where $\mathbf{x}_{R_r}(t)$ includes the quaternions and angular velocities of the target. However, the angular velocity of the target described in the target body-fixed frame needs to be expressed in the chaser body-fixed frame. It can be expressed in the chaser body-fixed frame by using the successive direction cosine matrices that transform from the target body-fixed frame to the chaser body-fixed frame. The transformed angular velocity of the target is given by

$$\boldsymbol{\omega}_c^t = C_{b_t}^{b_c} \boldsymbol{\omega}_t \quad (44a)$$

$$C_{b_t}^{b_c} = C_{N_I}^{b_c}\left(C_{N_I}^{b_t}\right)^T \quad (44b)$$

where $C_{N_I}^{b_c}$ and $C_{N_I}^{b_t}$ are the direction cosine matrices that describe the attitude of the chaser and the target with respect to the inertial reference frame, respectively.

V. State Estimation Using Extended Kalman Filter

To provide the robustness to the controllers in the presence of unmodeled process noises and the uncertainties of the plant parameters, the estimated states are used for the control computations. The estimated states can be compared to the true states so that they can meet the mission requirements if the precision sensors are available and the filters are properly designed. We assume the selected sensors can contribute to achieving the mission requirements of the close range rendezvous. We selected the EKF filter in this study for relative navigation and the chaser attitude estimation. The alternative nonlinear filters, such as an extended Kalman filter and a particle filter, can be replaced to obtain more improved and more stable estimation accuracy.

ISSN: 2277-3754
ISO 9001:2008 Certified
International Journal of Engineering and Innovative Technology (IJEIT)
Volume 3, Issue 2, August 2013

A. Relative Navigation

An EKF is used to sequentially estimate the relative position and velocity for relative navigation between two spacecrafts. We employed the sensor measurements of the RELAVIS system for precise relative navigation. The rendezvous laser vision (RELAVIS) system, designed by Optech and MD Robotics, is known to meet the navigation accuracy required for close range rendezvous. The RELAVIS system has the unique capability of producing highly accurate measurements over a range of 0.5 m to 5 km, providing range and bearing (azimuth and elevation angles) of the target with centimeter-level accuracy in range and about 0.02 degree in bearing [15]. The sensor specifications are shown in Table 1. The range, bearing accuracies, and FOV are of particular interest. Laser range-finder types of sensors, based on scanning the laser radar, have a limited FOV. In order to facilitate the use of RELAVIS, a one-hop V-bar approach of the chaser during the closing transfer is modified to three hops using the CW terminal guidance, leading to a possible application of RELAVIS so that the nominal approach trajectory meets the FOV constraint. The measurement errors are simulated as white Gaussian noise with a zero mean. The bias error is not included since the error is relatively small compared to the random errors and is ignored. The range-angles measurement model consisting of the range, azimuth and elevation angles is defined at t_k as

$$\mathbf{Y}_{pv,k}(\mathbf{x}_T,t)=\left[\sqrt{x^2+y^2+z^2}\quad \tan^{-1}\left(\frac{y}{x}\right)\quad \tan^{-1}\left(\frac{y}{x}\right)\right]^T+\boldsymbol{\varepsilon}_k \quad (45)$$

where $\boldsymbol{\varepsilon}_k$ is the measurement error vector. The errors are simulated as zero mean Gaussian noise. The applied standard deviation elements of $\boldsymbol{\varepsilon}_k$ are 5×10^{-2} m, 0.35 mrad and 0.35 mrad, respectively.

Table 1. RELAVIS sensor specifications

Minimum range	0.5 m
Maximum range	5 km
Field of View	±10 degrees
Maximum data sensing rate	8-10 kHz
Range Accuracy	1 cm
Bearing Accuracy	0.35 mrad

An EKF filter is used to sequentially estimate the relative position and velocity using the LIDAR system. The state for the relative navigation is identical to Eq. (26). For simple derivation, the partial derivative matrix of Eq. (6) to propagate the error covariance is given by

$$F_{pv}(\mathbf{x}_T(t))=\begin{bmatrix} 0 & 0 & 0 & 1 & 0 & 0 \\ 0 & 0 & 0 & 0 & 1 & 0 \\ 0 & 0 & 0 & 0 & 0 & 1 \\ \dot{f}^2+\frac{3\mu(r_t+x)^2}{r_c^5}-\frac{\mu}{r_c^3} & -2\dot{f}\frac{\dot{r}_t}{r_t}+\frac{3\mu y(r_t+x)}{r_c^5} & \frac{3\mu z(r_t+x)}{r_c^5} & 0 & 0 & 0 \\ 2\dot{f}\frac{\dot{r}_t}{r_t}+\frac{3\mu y^2 y(r_t+x)}{r_c^5} & \dot{f}^2+\frac{3\mu y^2}{r_c^5}-\frac{\mu}{r_c^3} & \frac{3\mu yz}{r_c^5} & -2\dot{f} & 0 & 0 \\ \frac{3\mu z(r_t+x)}{r_c^5} & \frac{3\mu yz}{r_c^5} & \frac{3\mu z^2}{r_c^5}-\frac{\mu}{r_c^3} & 0 & 0 & 0 \end{bmatrix} \quad (46)$$

The error covariance for the system process noise is given by

$$Q_{pv}=diag\left[0\quad 0\quad 0\quad \sigma_x^2\quad \sigma_y^2\quad \sigma_z^2\right] \quad (47)$$

where σ_x,σ_y, and σ_z are the spectral densities of the process noise components given by $10^{-7}m/(s\sqrt{s})$. The error covariance corresponding to LIDAR measurements is given by

$$R_{pv}=diag\left[\sigma_r^2\quad \sigma_b^2\quad \sigma_b^2\right] \quad (48)$$

where the measurement standard deviations of σ_r and σ_b are given by 0.35 mrad and 5 cm. The matrices F and Q_L are used for covariance propagation. By taking the partial derivative of the measurement vector, the measurement sensitivity matrix at t_k is given by

$$H_{pv}(\mathbf{x}(t_k))=\begin{bmatrix} \frac{x}{r} & \frac{y}{r} & \frac{z}{r} & 0 & 0 & 0 \\ -\frac{y}{\sqrt{x^2+y^2}} & \frac{x}{\sqrt{x^2+y^2}} & 0 & 0 & 0 & 0 \\ -\frac{xz}{r^2\sqrt{x^2+y^2}} & -\frac{yz}{r^2\sqrt{x^2+y^2}} & \frac{\sqrt{x^2+y^2}}{r^2} & 0 & 0 & 0 \end{bmatrix} \quad (49)$$

The EKF filter with the RELAVIS scanning measurement system can now be used with these quantities to estimate the relative attitude, position and velocity.

B. Attitude Estimation

An EKF filter is used to sequentially estimate the attitude and angular rate of a chaser with three axis gyroscopes (gyros) and "quaternion out" star trackers. Among the several parameterizations, such as Euler angles, quaternions, modified Rodrigues parameters, chosen to represent the attitude, quaternions are selected. Quaternions are appealing since no singularities are present and the kinematic equation is bilinear. However, the quaternion must obey a normalization constraint, which can be violated by the linear measurement updated with the standard EKF approach. To overcome this

ISSN: 2277-3754
ISO 9001:2008 Certified
International Journal of Engineering and Innovative Technology (IJEIT)
Volume 3, Issue 2, August 2013

drawback, a multiplicative error quaternion in the body frame, where after neglecting higher-order terms, is used. The four-component quaternion can effectively be replaced by a three-component error vector [15]. A combined quaternion from two star trackers is assumed for the measurement. To generate synthetic measurements, the following model is used: [16]

$$\tilde{\mathbf{q}} = \begin{bmatrix} 0.5\nu \\ 1 \end{bmatrix} \otimes \mathbf{q} \tag{50}$$

is used where $\otimes$ denotes quaternion multiplication. The variable $\tilde{\mathbf{q}}$ is the quaternion measurement, $\mathbf{q}$ is the truth, and ν is the measurement noise, which is assumed to be a zero-mean Gaussian noise process with a covariance of $0.001 I_{3\times3}\,\text{deg}^2$. An error quaternion between the measured quaternion and the estimated quaternion is used for measurement in the filter. This is computed using

$$\delta\mathbf{q} = \begin{bmatrix} \delta q_1 & \delta q_2 & \delta q_3 & \delta q_4 \end{bmatrix}^T = \tilde{\mathbf{q}} \otimes \hat{\mathbf{q}}^{-1} \tag{51}$$

For small angles, the vector portion of the quaternion is approximately equal to half angles so that $\delta q_{i=1,2,3} \approx \delta\boldsymbol{\alpha}/2$ and $\delta q_4 \cong 1$. The vector $\delta\boldsymbol{\alpha}$ has components of roll, pitch, and yaw error angles that are independent of rotation sequence. A common sensor that measures the angular rate is a rate-integrating gyroscope[5]. For this sensor, a widely used model is given by

$$\tilde{\boldsymbol{\omega}} = \boldsymbol{\omega} + \boldsymbol{\beta} + \boldsymbol{\eta}_v \tag{52a}$$

$$\dot{\boldsymbol{\beta}} = \boldsymbol{\eta}_u \tag{52b}$$

where $\tilde{\boldsymbol{\omega}}$ is the continuous-time measured angular vector and $\boldsymbol{\omega}$ is the time propagation of the angular dynamics in Eq. (19). $\boldsymbol{\beta}$ is the bias vector and $\boldsymbol{\eta}_v$ and $\boldsymbol{\eta}_u$ are independent zero-mean Gaussian white noise processes with

$$E\left\{\boldsymbol{\eta}_v(t)\boldsymbol{\eta}_v^T(t)\right\} = I_{3\times3}\sigma_v^2\delta(t-\tau) \tag{53a}$$

$$E\left\{\boldsymbol{\eta}_u(t)\boldsymbol{\eta}_u^T(t)\right\} = I_{3\times3}\sigma_u^2\delta(t-\tau) \tag{53b}$$

where $\delta(t-\tau)$ is the Dirac delta function. For the design of an attitude filter based on EKF, the linearized model regarding multiplicative quaternion formulation is employed by

$$\Delta\dot{\tilde{\mathbf{x}}}(t) = F_q(\tilde{\mathbf{x}}(t),t)\Delta\tilde{\mathbf{x}}(t) + G_q(t)\mathbf{w}_q(t) \tag{54}$$

where

$\Delta\tilde{\mathbf{x}}_q(t) = \begin{bmatrix} \delta\boldsymbol{\alpha}^T(t) & \delta\boldsymbol{\beta}^T(t) \end{bmatrix}^T$, $\mathbf{w}_q(t) = \begin{bmatrix} \boldsymbol{\eta}_v^T(t) & \boldsymbol{\eta}_u^T(t) \end{bmatrix}^T$, $F_q(\hat{\mathbf{x}}_q(t),t)$, $G_q(t)$ and $Q_q(t)$ are given by

$$F_q(\hat{\mathbf{x}}_q(t),t) = \begin{bmatrix} -[\hat{\boldsymbol{\omega}}_c\times] & -I_{3\times3} \\ 0_{3\times3} & 0_{3\times3} \end{bmatrix} \tag{55a}$$

$$G_q(t) = \begin{bmatrix} -I_{3\times3} & 0_{3\times3} \\ 0_{3\times3} & I_{3\times3} \end{bmatrix} \tag{55b}$$

The discrete process noise covariance [17] is given by

$$Q_q(t_k) = \begin{bmatrix} (\sigma_v^2\Delta t + \frac{1}{3}\sigma_u^2\Delta t^2)I_{3\times3} & (\frac{1}{2}\sigma_u^2\Delta t^2)I_{3\times3} \\ (\frac{1}{2}\sigma_u^2\Delta t^2)I_{3\times3} & (\sigma_u^2\Delta t)I_{3\times3} \end{bmatrix} \tag{56}$$

where the noise parameters for the gyro measurements are given by $\sigma_u = \sqrt{10}\times10^{-10}$ rad/sec$^{3/2}$ and $\sigma_v = \sqrt{10}\times10^{-5}$ rad/sec$^{1/2}$. The initial bias for each axis is given by 0.1 deg/hr. Also, the gyro measurements are sampled at the same rate as the star tracker measurements. The initial covariance for the attitude error is set to 0.1^2 deg^2, and the initial covariance for the gyro drift is set to 0.2^2 (deg/hr)^2. These quantities are converted in radians and given by $P_{q_0}^a = 3.0642\times10^{-6}$ and $P_{q_0}^b = 9.4018\times10^{-13}$.

$$P_{q_0} = diag\begin{bmatrix} P_{q_0}^a & P_{q_0}^a & P_{q_0}^a & P_{q_0}^b & P_{q_0}^b & P_{q_0}^b \end{bmatrix} \tag{57}$$

The error covariance corresponding to star tracker measurements is given by

$$R_q = diag\begin{bmatrix} \sigma_q^2 & \sigma_q^2 & \sigma_q^2 \end{bmatrix} \tag{58}$$

where σ_q is 0.001 degrees. The measurement residual vector for the EKF sequence is computed through the error quaternion in Eq. (51) instead of the conventional difference between the measurement and the estimated output.. Thus, the measurement residual vector in the EKF filter is newly given by $\delta\boldsymbol{\alpha}/2$. The final part in the EKF involves the quaternion and bias updates. The error-state update at t_k is the multiplication of the Kalman gain and the measurement residual using the error quaternion as follows:

$$\Delta\hat{\mathbf{x}}_k^+(t) = K_k\delta\boldsymbol{\alpha}(t)/2 \tag{59}$$

where K_k is the Kalman gain at t_k. The sensitivity matrix at t_k is then given by

$$H_q(\hat{\tilde{\mathbf{x}}}_k^-) = \begin{bmatrix} \frac{1}{2}I_{3\times3} & 0_{3\times3} \end{bmatrix} \tag{60}$$

The gyro bias update at t_k is simply given by

$$\hat{\boldsymbol{\beta}}_k^+ = \hat{\boldsymbol{\beta}}_k^- + \Delta\hat{\boldsymbol{\beta}}_k^+ \tag{61}$$

ISSN: 2277-3754
ISO 9001:2008 Certified
International Journal of Engineering and Innovative Technology (IJEIT)
Volume 3, Issue 2, August 2013

The angular velocity is propagated by

$$\hat{\boldsymbol{\omega}}(t) = \tilde{\boldsymbol{\omega}}(t) - \hat{\boldsymbol{\beta}}(t) \tag{62}$$

The quaternion update is more complicated. As previously mentioned, the fourth component of $\delta\mathbf{q}$ is nearly one. Therefore, to first-order the quaternion update, at t_k is given by

$$\hat{\mathbf{q}}_k^+ = \begin{bmatrix} \frac{1}{2}\delta\hat{\boldsymbol{\alpha}}_k^+ \\ 1 \end{bmatrix} \otimes \hat{\mathbf{q}}_k^- \tag{63}$$

VI. Numerical Results and Analysis

The target and the chaser vehicles are selected as the automatic transfer vehicle (ATV) of ESA and international space station (ISS), respectively, for the application of close range rendezvous and docking phases. Six-degrees-of-freedom simulation for the translational and rotational maneuvers required for close range rendezvous were established to demonstrate the performance of the proposed controllers. The simulation scenario assumed that the target center of mass is located at the origin of the inertial coordinate with zero velocity, as illustrated in Fig. 1. The chaser (ATV) is initially positioned at a position of $[0.2\ -2500\ 0.1]^T$ *m* with respect to the target center of the mass in the CW frame. The initial relative velocity in the CW frame is $[-0.01\ 0.432\ 0.01]^T$ m/s. While the body frame of the target is assumed to be coincided with the CW frame, the initial attitude of the chaser is rotated by 120 degrees of roll, -50 degrees pitch and 20 degrees of yaw in a 3-2-1 rotation sequence with respect to the target body frame. The corresponding chaser quaternion is then given by

$$\mathbf{q}_c(t_0) = [\,0.4391 \quad -0.0718 \quad 0.8097 \quad 0.3827\,]^T \tag{64}$$

The target is assumed to maintain a constant attitude for docking with the chaser. The initial mass of the chaser is assumed as the ATV's launch mass of 19,600 kg, and is time varying as the propellant is consumed. The propellant consumption is assumed to be known. The moment of inertia [2] and the chaser moment of matrix [18] are respectively given by

$$I_t = 10^6 \times \begin{bmatrix} 128 & 0 & 0 \\ 0 & 107 & 0 \\ 0 & 0 & 201 \end{bmatrix}, \quad I_c = 10^6 \times \begin{bmatrix} 1.091 & -0.027 & -0.008 \\ -0.027 & 8.287 & -0.328 \\ -0.008 & -0.328 & 0.328 \end{bmatrix} kg \cdot m^2 \tag{65}$$

The quaternions of the target, $\mathbf{q}_t$, are generated using Eq. (7) after replacing the subscript *t* with *c* with the constant angular velocity of $\boldsymbol{\omega} = [0 \quad 0.0011 \quad 0]^T$ rad/s, which corresponds to an Earth-pointing target. The initial angular velocity of the chaser spacecraft is given by $\boldsymbol{\omega}_c(t_0) = 0_{3\times1}$. The target is assumed to have the following orbital elements described in Table 2 below.

Table 2. Orbital elements of the target

Semi major axis	6739.188 km
Eccentricity	0.0005817
Inclination	51.64 deg.
Right ascension ascending node	316.44 deg.
Argument of perigee	40.90 deg.
Mean anomaly	319.24 deg.

The objectives of the controls are to have the center of the mass of the chaser be positioned at a position of $[0\ -20\ 0]^T$ *m* in the CW frame with a slow approach speed and its attitude to be coincided with the target body frame. Originally, a closing transfer is initiated in the starting point to bring ATV to a point, 250 *m*, behind the docking port. However, it is modified to three times of V-bar hops so that a RELAVIS system can be used for satisfying a field of view, as shown in Table 1. Close range rendezvous phases are then composed of three times of V-bar hops from the starting point, two times of station keeping, and a straight line V-bar maneuver to the desired position. Thus, the chaser spacecraft is required to perform a series of translational maneuvers composed of complicated position changes, as well as a large angle maneuver. As a result, the simulation for translational and rotational maneuvers was performed for 91 minutes by a 0.1 second step size until the chaser satisfied the conditions for docking phase from the 2500 m away starting point.

The state estimations using EKF filters are also simultaneously performed to provide the real time state variation to the controllers. The robustness of the proposed control system was tested by imposing external disturbances, and the plant uncertainties of varying mass and moment of inertia. The external disturbances were modeled by white Gaussian noise with identical spectral densities of the process noise in Eq. (47). The fixed initial chaser mass was used to command control forces whereas the "truth" real mass was varied by using the time rate of consumption of the propellant. This study assumes the mass variation by translational maneuvers only for simplification. The consumed propellant mass is given by

$$\Delta m = \frac{\|\mathbf{F}\| \cdot \Delta t}{I_{sp} \cdot g_0} \tag{66}$$

Where, I_{sp} is the specific impulse and the employed value is 280 in seconds. g_0 is the acceleration at the Earth's surface and Δt is time step. And $\|\mathbf{F}\|$ is the applied control force magnitude. The uncertainty of the moment of the inertia was also applied by adding ΔI_c to I_c when the chosen ΔI_c is equal to 30% of I_c. The control torques are then commanded with the added moment of the inertia instead of the original chaser moment of inertia, I_c. All of numerical simulation results were achieved in the external disturbances and the uncertainties of the plant parameters. Figure 3 (a) shows the overall close range rendezvous trajectory from the starting point to the target docking port with successful tracking of the desired

ISSN: 2277-3754
ISO 9001:2008 Certified
International Journal of Engineering and Innovative Technology (IJEIT)
Volume 3, Issue 2, August 2013

nominal trajectory meeting the final conditions [19] in Table 3 to be reached at docking phase. It is critical to ensure that the chaser enters the approach corridor and passes through it without crossing keep-**o**ut zone in the final straight line approach. Figure 3 (b) shows that it safely entered within ±5 degrees of the approach corridor after performing two times of station keepings in the keep-out zone. The controlled trajectory shows that it satisfies this constraint. Figure 4 presents the entire close range rendezvous trajectory in three dimensional spaces. Figure 5 shows the controlled relative position with respect to the desired nominal relative position. The controlled trajectory in Fig. 5 tracks the nominal trajectory with satisfying translational conditions required for docking phase.

Translational Conditions		Rotational Conditions	
Relative longitudinal closing velocity	0.05~0.10 m/s	Misalignment angles	< 5 deg
Relative lateral velocity	< 0.02 m/s	Angular rate (roll)	< 0.40 deg/s
Lateral misalignment	< 0.1 m	Angular rate (pitch)	< 0.15 deg/s

Table 3. Conditions for successful docking (3σ)

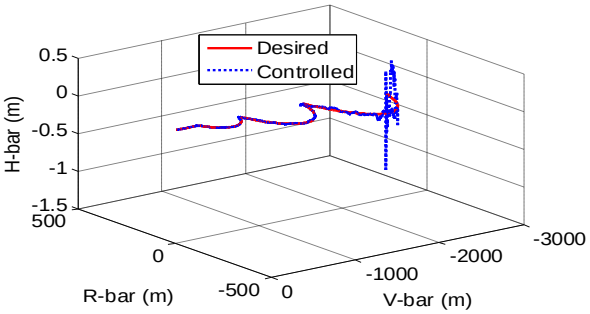

Fig. 4. Proximity operations in 3-D spaces

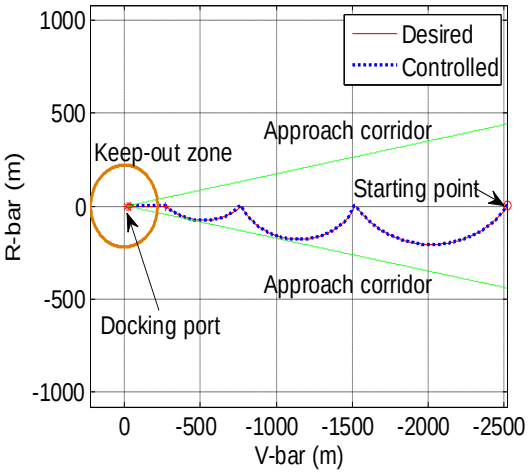

Fig. 3. (a) Overall close range rendezvous trajectory.

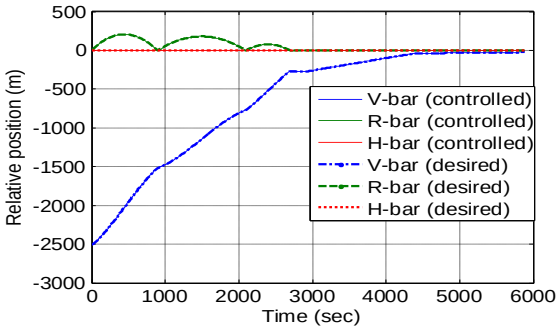

Fig. 5. Relative position history

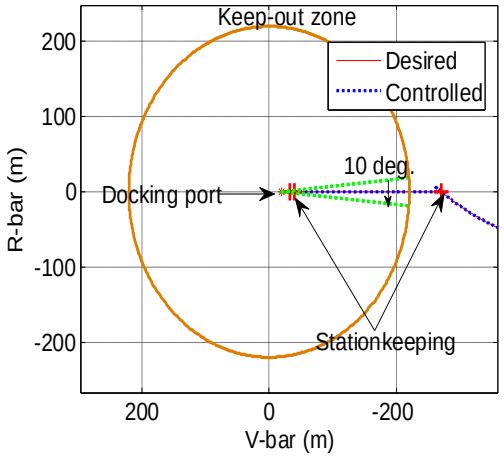

Fig. 3. (b) Final V-bar approach trajectory.

It is important to note that the relative position and velocity tracking errors, and approach velocity histories, in Figs. 6 and 7 are used to ensure that the docking conditions are satisfied. After the chaser performed the final station keeping in the straight V-bar approach, its position tracking error was maintained by less than 0.07 *m* to the docking port and satisfied the lateral misalignment condition that is less than 0.1 *m*. The relative velocity history along each direction, shown in Figure 7, was less than 0.07 *m/s* and satisfies the longitudinal closing and lateral velocity conditions during the straight line approach. Whenever the controller reinitialized at each assigned point of the subsequent phase, the applied control forces exhibits large impulsive reactions but they never surpass the maximum thrust as shown in Figure 8.

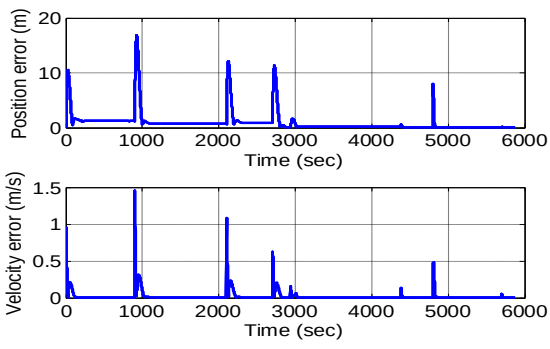

Fig. 6. Tracking errors history

ISSN: 2277-3754
ISO 9001:2008 Certified
International Journal of Engineering and Innovative Technology (IJEIT)
Volume 3, Issue 2, August 2013

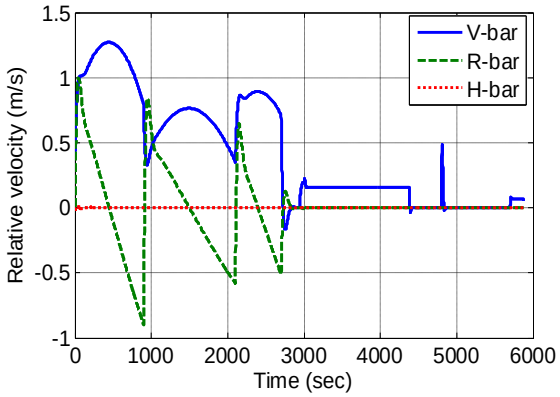

Fig. 7. Approach velocity history

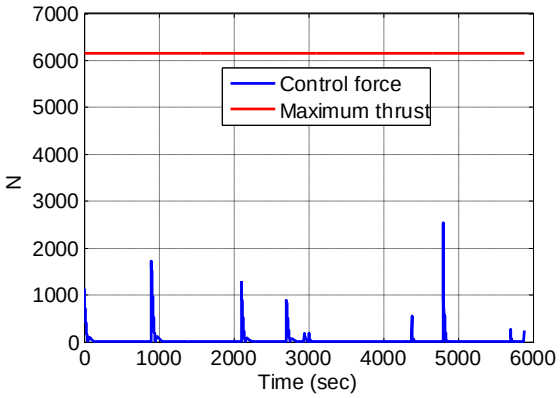

Fig. 8. Control force history

Figure 9 presents the propellant mass consumption while the control forces were applied. Thus, the robustness of the controller for the translational maneuver was tested simultaneously by employing the uncertainty of the mass, 19,600 kg of the "uncertain," fixed mass, whereas the actual ("truth") mass variation considering the consumed propellant mass was employed in the EKF filter.

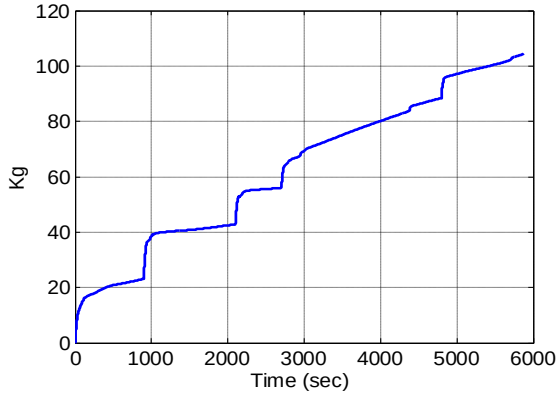

Fig. 9. Propellant mass consumption

Figures 10 and 11 show the relative position and velocity estimation errors with respect to the true values. Relative position knowledge is within 0.1 *m* for each direction. And relative velocity knowledge is in within 1×10^{-4} m/s for each direction. The momentary rise in the velocity error around 4500 sec was caused by the first station keeping command to remove out relative velocity. These precise estimation results contributed to from the better control forces.

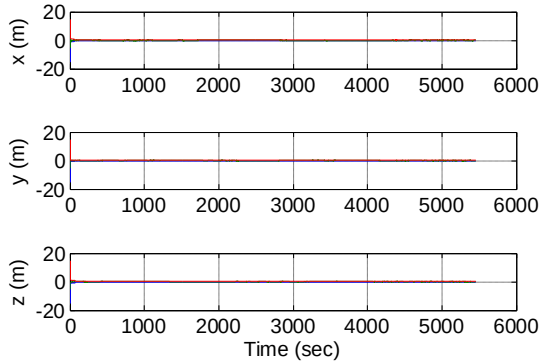

Fig. 10. Relative position errors and 3 σ bounds

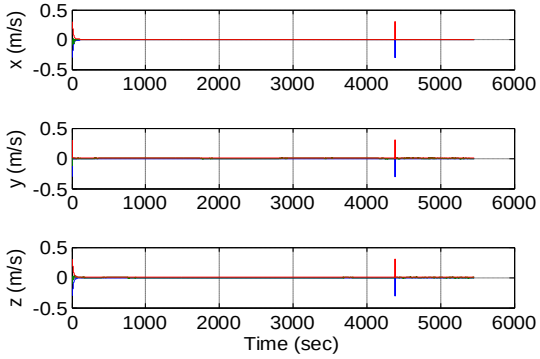

Fig. 11. Relative velocity errors and 3 σ bounds

The robustness of the attitude controller was also evaluated in the presence of uncertainty of the moments of inertia. The uncertainty was quantified by adding 30 percent of the moment of inertia to the initial value. Additionally, random external disturbances, which were not modeled in the controller, were included as modeled in the Euler rotational equation of motion in Eq. (19) for "the selected truth model". Using the initial conditions given in Eq. (64), the chaser successfully performs a rotational maneuver so that the chief body axis can coincide with the target body axis. Thus, the objective of a rotational maneuver is to achieve $[0\ 0\ 0\ 1]^T$ quaternion error between the target and the chaser. Figure 12 presents the modeled external disturbance torques history to evaluate the robustness of the controller. The upper graph in

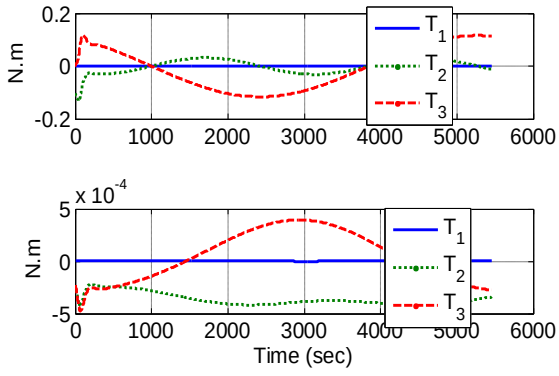

Fig. 12. External disturbance torques history

Figure 12 shows the gravity-gradient torque history and the lower graph shows the random external disturbance torque

ISSN: 2277-3754
ISO 9001:2008 Certified
International Journal of Engineering and Innovative Technology (IJEIT)
Volume 3, Issue 2, August 2013

history. Figure 13 presents the Euler angle error history between the target and the chaser body axes from the starting point to docking phase. The chaser could achieve attitude tracking errors less than 1 degree in 300 seconds and then maintain tracking error less than 0.1 degrees to docking phase even in external disturbances and uncertainty of the moments of inertia.

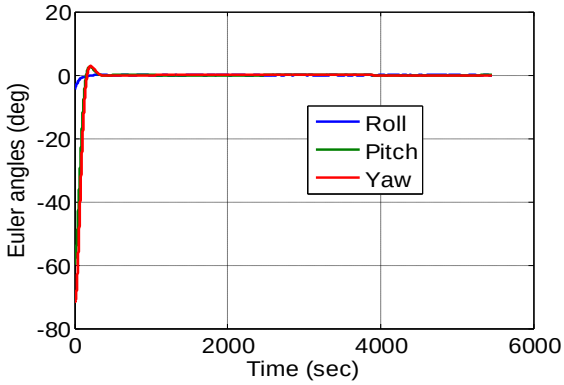

Fig. 13. Euler angle error history

Figure 14 shows that the chaser tracks the target's attitude rate, which corresponds to an Earth-pointing spacecraft. Obviously, the desired angular velocity motion is achieved. Thus, Figs. 13 and 14 demonstrate that the important rotational conditions for docking phase in Table 2 are successfully met. Figures 15 and 16 present that the property of attitude matching expressed in quaternions whose values converge to the desired value and the norm of attitude error. Figure 17 shows the applied control torque history whose values are reasonable to maintain the desired attitude tracking.

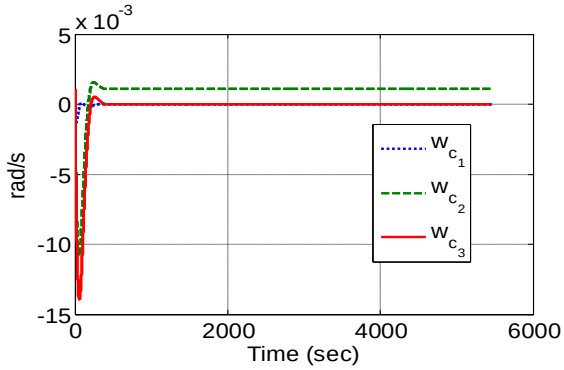

Fig. 14. Angular rate history

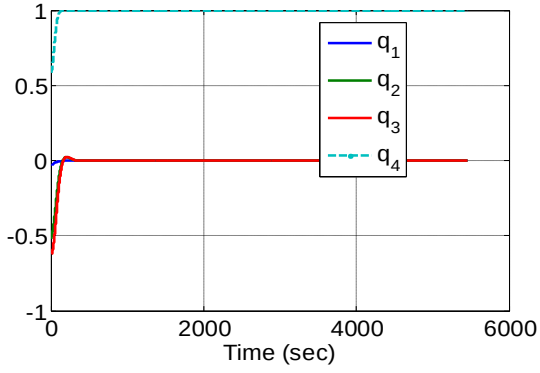

Fig. 15. Quaternion error history

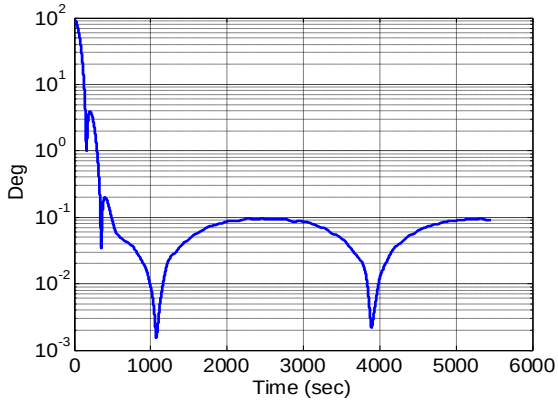

Fig. 16. Norm of attitude error

The attitude estimation and 3σ bounds using the EKF are shown in Fig. 18. The attitude estimation results sufficiently meet the conditions for rotational maneuvers for docking phase. A plot of the gyro drift estimates are also shown in Fig. 19. The y and z axes have large response due to the large pitch and yaw maneuvers. This estimation results clearly show the EKF can be combined with the SDRE control method to achieve effective and robust rotational maneuver or attitude tracking. This robustness in this example could be obtained by the support of precisely the EKF filter-based estimated states using quaterinion producing star trackers and gyroscope measurements. As matter of the fact, the estimated states contribute to form the control values so that the control state can be comparable to the true state with allowable errors to satisfy the control objectives.

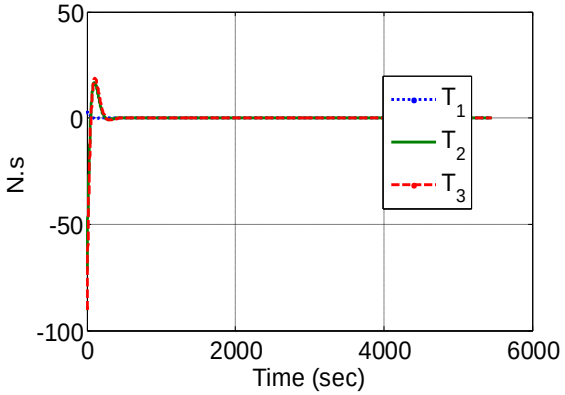

Fig. 17. Control torque history

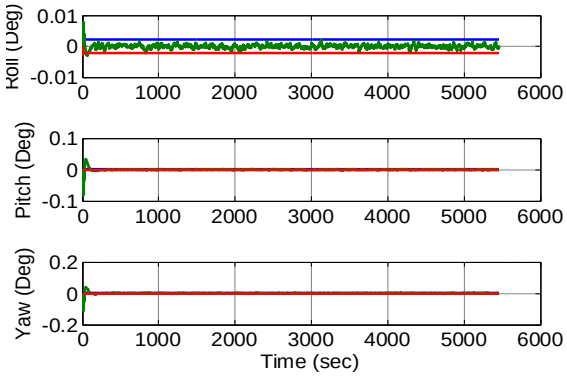

Fig. 18. Attitude errors and 3 σ bounds

ISSN: 2277-3754
ISO 9001:2008 Certified
International Journal of Engineering and Innovative Technology (IJEIT)
Volume 3, Issue 2, August 2013

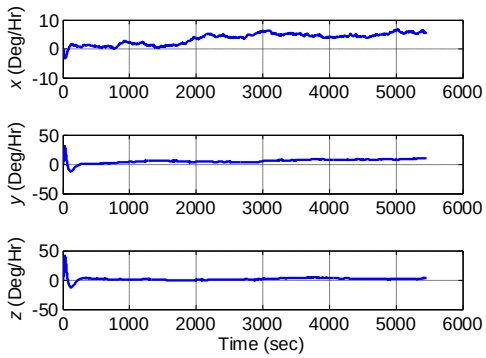

Fig. 19. Gyro drift estimates

VII. CONCLUSION

The robust full state feedback control technique was presented using the combination the state-dependent Riccati equation (SDRE) control and the extended Kalman filter to perform close range rendezvous and docking phases which require precise translational and rotational maneuvers. The unified state-dependent Riccati equation (SDRE) method was used to design both the position and attitude controllers. Then, nonlinear state feedback controllers via the estimated states using extended Kalman filters which estimate both the position and attitude were designed.

A six-degree-of freedom simulation was utilized to demonstrate excellent tracking performance in the presence of external disturbances and the uncertainties of plant parameters. Simulation results demonstrated the robust full state feedback control method could successfully perform close range rendezvous and satisfy the translational and rotational conditions required for docking phase.

REFERENCES

[1] Goodman, J. L., Brazzel, J. P., and Chart, D. A., "Challenges of Orion Rendezvous Development,"AIAA Guidance, Navigation and Control and Exhibit, South Carolina, August 20-23, 2007. J. U. Duncombe, "Infrared navigation—Part I: An assessment of feasibility," IEEE Trans. Electron Devices, vol. ED-11, pp. 34-39, Jan. 1959.

[2] C. Y. Lin, M. Wu, J. A. Bloom, I. J. Cox, and M. Miller, "Rotation, scale, and translation resilient public watermarking for images," IEEE Trans. Image Process., vol. 10, no. 5, pp. 767-782, May 2001.

[3] Stansbery, D.T. and Cloutier, J.R., "Position and Attitude Control of a Spacecraft Using the State Dependent Riccati Equation Technique," Proceedings of the American Control Conference, Chicago, IL, June, 2000.

[4] T. Cimen, "Survey of State-Dependent Riccati Equation in Nonlinear Optimal Feedback Control Synthesis," Journal of Guidance, Control and Dynamics, Vol. 35, No.4, 2012, pp. 1025-1047.

[5] T. Cimen, "Systematic and Effective Design of Nonlinear Feedback Controllers via the State-Dependent Riccati Equation Method," Annual Reviews in Control, Vol. 34, No. 1, 2010, pp. 32-51.

[6] Parrish, D.K., and Ridgely, D.B., "Attitude Control of a Satellite Using SDRE Method," Proceedings of the American Control Conference, 1997, pp. 942–945.

[7] Wise, K.A., and Sedwick, J.L., "Nonlinear Control of Agile Missiles Using State Dependent Riccati Equations," Proceedings of the American Control Conference, 1997, pp. 379–380.

[8] Cimen, T., "State-Dependent Riccati Equation (SDRE) Control: A Survey," Proceedings of the 17th World Congress, The International Federation of Automatic Control, Seoul, Korea, July 6-11, 2008.

[9] Atassi, A. N. and Khalil, H. K., A Separation Principle for the Control of a Class of Nonlinear Systems, IEEE Transactions on Automatic Control, Vol. 46, No. 5, MAY 2001, pp. 742-746.

[10] Lewis, L. F. and Syrmos., V. L., Optimal Control, 2nd edition, John Wiley and Sons, Inc., 1995,

[11] Crassidis, J. L., and Junkins, J. L., Optimal Estimation of Dynamic Systems, a CRC Press Company, 2004.

[12] Schaub, H. and Junkins, J. L., Analytical Mechanics of Aerospace Systems, American Institute of Aeronautics and Astronautics, Inc., New York, NY., 2003.

[13] Prussing, J.A. and Conway, B. A., Orbital Mechanics, Oxford University Press, Inc., Avenue, New York, pp. 164 -168, 1993.

[14] Madonna, R. G., Orbital Mechanics, Kriger Publishing Company, Inc., pp. 105-107, 1997.

[15] Pelletier, F.J. and Golla, D.F., "Lidar-Based Rendezvous Navigation for MSR," AIAA/AAS Astrodynamics Specialist Conference and Exhibit, Providence, Rhode Island, August 2004.

[16] Lefferts, E.J, Markley, F.L. and Shuster, M.D., "Kalman Filtering for Spacecraft Attitude Estimation," Journal of Guidance, Control, and Dynamics, Vol. 5, No. 5, Sept.-Oct. 1982, pp. 417-429.

[17] Crassidis, J.L. and Junkins, J.L., Optimal Estimation of Dynamic Systems, Chapman and Hall/CRC, 2004.

[18] Nagata, T., Modi, V. J. and Matsuo, H. "Dynamics and Control of Flexible Multibody Systems Part II: Simulation Code and Parametric Studies with Nonlinear Control," Acta Astronautica, Vol. 49, No. 11, 2001, pp. 595–610.

[19] Pinard, D., Reynaud, S., Delpy, P. and Strandmoe, S.E., "Accurate and Autonomous Navigation for the ATV," Aerospace Science and Technology, pp. 490–498, September, 2007.

AUTHOR BIOGRAPHY

Daero Lee worked at the division of aerospace engineering school of mechanical, aerospace & systems engineering, KAIST, Daejeon, Korea as a postdoc researcher in 2011. He received the Ph.D. degree in aerospace engineering in 2009 from Missouri University of Science and Technology, Rolla, Missouri, USA. His research interests include astrodynamics, spacecraft dynamics, control and estimation, spacecraft formation flying, spacecraft hovering around the asteroid, and spacecraft trajectory optimization.

ISSN: 2277-3754
ISO 9001:2008 Certified
International Journal of Engineering and Innovative Technology (IJEIT)
Volume 3, Issue 2, August 2013

Hyochoong Bang is the professor at the division of aerospace engineering school of mechanical, aerospace & systems engineering, KAIST, Daejeon, Korea. He received the Ph.D. degree in aerospace engineering in 1992 from Texas a&M, College Station, Texas, USA. He has published several papers on spacecraft GNC, and UAV. His research interests include spacecraft GNC algorithm, spacecraft attitude control and determination, and spacecraft and UAV related system developments.